49th AIAA Aerospace Sciences Meeting including the New Horizons Forum and Aerospace Exposition
4 - 7 January 2011, Orlando, Florida

AIAA 2011-906

Electrical and optical study of DC driven repetitively pulsed transient spark discharge in atmospheric air

Mario Janda *, Zdenko Machala †, and Viktor Martisovits ‡
Division of Environmental Physics
Faculty of Mathematics, Physics and Informatics, Comenius University
Mlynska dolina F2, 84248 Bratislava, Slovakia
e-mail: machala@fmph.uniba.sk

We present a study of electrical properties and optical emission of transient spark (TS) - streamer-to-spark transition discharge in atmospheric pressure air. TS was succesfully applied for flue gas cleaning or bio-decontamination and has a potential in plasma shielding, combustion, and flow control applications. Despite the DC applied voltage, TS has a pulsed character with short ($\sim$10 –100 ns) high current (>1 A) pulses, with repetitive frequencies 1–20 kHz. Estimation of the temporal evolution of electron density n_e using discharge diameter measured by time-resolved iCCD imaging, supported by preliminary spectroscopic n_e measurements from H_α broadening, show that $n_e \approx 10^{16}$-10^{17} cm^{-3} at maximum and $\sim 10^{11}$ cm^{-3} in average are reached using relatively low power delivered to the plasma (0.2–3 W). Thanks to the high repetition frequency, n_e between two current pulses does not fall below a critical value and therefore plasma exists during the whole time. A detailed analysis of the TS control by electrical circuit parameters is presented. With appropriate circuit components, the current pulse tail (>1 mA) can be extended and the electron density can be held above $\sim 10^{13}$ cm^{-3} for several tens of μs.

I. Introduction

Atmospheric pressure non-thermal plasmas in air generated by electrical discharges present considerable interest for a wide range of environmental, bio-medical and industrial applications, such as air pollution control, waste water cleaning, bio-decontamination and sterilization, or material and surface treatment [1–6]. In all of these applications, the desired chemical effect is achieved by efficient production of reactive radicals in non-thermal plasma. The key factor for their production are high energy electrons, which can be accelerated by electric field to reach energies of several eV, while the background gas remains cold.

The simplest approach to generate atmospheric pressure plasma is applying a DC constant voltage on a couple of metal electrodes. If the generated electric field is non homogeneous thanks to the geometry of electrodes, e. g. pin-to -plane configuration, a gradual increase of the onset voltage will lead to the generation of corona or streamer corona discharge [7]. Streamers are filamentary structures propagating towards the grounded electrode. Very strong reduced electric field strengths *E/N* ($\sim$600 Td) and high electron densities n_e ($\sim 10^{14}$ cm^{-3}) can be reached in their head [8]. Streamers can therefore significantly influence the plasma-induced chemistry. However, streamers can also lead to the transition to spark or arc discharge [7,9], generating thermal plasma. Much more power is required to sustain these discharges and the high energy cost allow their utilization only for applications, where one can either expect valuable products (e. g. H_2) or needs to completely destroy very dangerous pollutants [10–12].

Two of the most common ways of disabling streamer-to-spark transition are based on covering at least one electrode by an insulator (e. g. dielectric barrier discharge) or by using very short high voltage (HV) pulses. We will only discuss in more detailes the second approach, since it is more relevant to discharge described in this paper.

It was found that formation of active species depends on the maximum applied voltage (10 –20 kV/cm), voltage rise time (up to 10 ns), decay time (<1–10 μs) and total duration of the HV pulse (<0.1 μs) [13–16]. The increasing repetition frequency of the HV pulses up to 200 Hz also showed an improved efficiency of removal of various pollutants [16]. HV pulsed devices working at repetition frequencies above 1 kHz appeared only recently [17–20]. The importance of the high repetition frequency on power efficiency of the plasma generation was emphasized [18–20]. The 'spark' regime of nanosecond repetitive pulse discharge operating at frequency 30 kHz in air preheated to 1000 K, which was already successfully used for stabilization of lean flames [21], was shown to generate plasma with peak electron density $\sim 10^{15}$ cm^{-3}, while consuming only 0.2–1 mJ per pulse [20]. The only disadvantage of this method could be the price of the HV pulse generator.

*Researcher.
†Associate Professor, Senior AIAA Member.
‡Professor.

A restriction of thermal plasma generation when using a DC power supply, can be simply achieved by adding a ballast resistor ($R > 1\,\mathrm{M\Omega}$) between the high voltage (HV) electrode and the DC power supply. Since R will limit the average discharge current to several mA, streamer corona will be transformed to either high pressure glow discharge (GD) or transient spark (TS), depending on the gas composition, flow rate, value of R and geometry of electrodes [22–24]. The high pressure glow discharge has already been applied e. g. for flue gas cleaning [22,25] and it has a great potential for other applications, such as plasma shielding, since it is a source of stable scalable plasma where $n_e \approx 10^{12}\,\mathrm{cm}^{-3}$ can be achieved.

TS discharge regime was first mentioned in [22] and further described in [24]. TS is therefore still a relatively new type of discharge, yet its concept is similar to the prevented spark studied in the group of Marode [26–28]. Periods with TS were also observed by Akishev et al. [29], while studying instabilities of GD due to a fast gas flow. TS is a filamentary streamer-to-spark transition discharge initiated by a streamer, which transforms to a short spark pulse due to the discharging of the internal capacity C of the reactor. TS is based on charging and discharging of C. For typical R and C ($\sim$10 pF), a repetition frequency of this process 1–20 kHz can be achieved. TS represents a simple solution to generate short ($\sim$10 –100 ns) high current pulses ($\sim$1–10 A) with high repetition frequency ($\sim$kHz). Thanks to the short current pulse duration, the plasma generated by TS has different properties than the plasma generated by an ordinary spark. Our previous time-integrated emission spectroscopy study showed that TS pulses generate highly reactive nonequilibrium plasma with excited atomic radicals (O*, N*), excited molecules N_2* and ions N_2^+*, and gas temperature T_g ranging from 500 to 1500 K, while vibrational temperature T_v was from about 3800 K to 5000 K [5]. In comparison with an ordinary spark (or even high pressure glow discharge) TS has also relatively low power budget: the discharged energy in one TS pulse is small ($\sim$0.1–1 mJ) and the total power, depending on pulse frequency, is 0.1–2 W. [5,22].

Thanks to these characteristics, TS is not applicable where heating to even just about 500 K can be harmful, e. g. for treatment of heat sensitive solid materials, but is applicable for flue gas cleaning or bio-decontamination, and has a potential in plasma shielding, combustion, and flow control applications. Various applications have different demands on TS with respect to the optimal frequency, energy per pulse, etc. So the optimization of TS for various applications and better ability to control it by changing electric circuit parameters requires further research.

II. Experimental setup

Figure 1 shows a simplified scheme of the experimental set-up. Experiments were carried out at room temperature in atmospheric pressure air with a gas flow perpendicular to discharge channel with a velocity $\sim$0.2 m.s^{-1}. A stainless steel hypodermic needle (20G$\times 1^1/_2$", 0.9$\times$40 mm) with standard bevel was used as a high voltage (HV) electrode opposite to a grounded planar copper electrode. The distance between electrodes d = 5 mm.

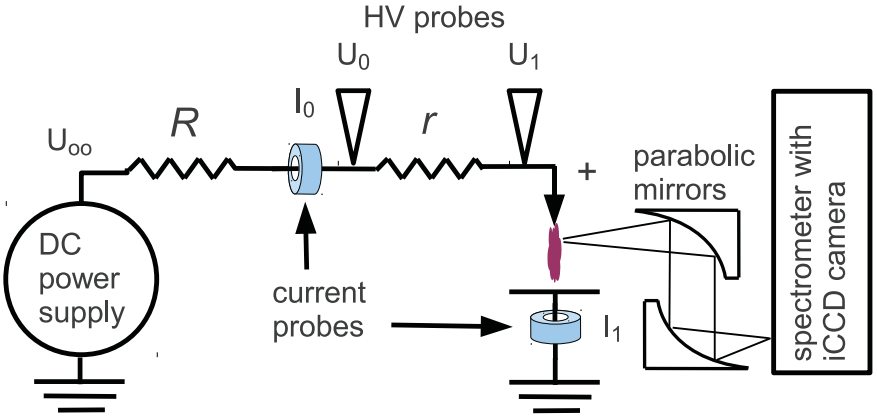

Figure 1. Simplified scheme of the experimental set-up.

A DC High Voltage (HV) power supply connected via a series resistor *R* limiting the total current was used to generate a positive TS discharge. The value of *R* varied from 3.5 to 9.84 MΩ. Additional small resistor *r*, the effect of which we further studied, was attached directly to the HV electrode, separating it thus from a HV cable connecting it with the resistor *R* (Fig. 1). The value of *r* varied from 0 (no *r*) to 110 kΩ.

The discharge voltage was measured by two 100 MΩ high voltage probes (Tektronix P6015A) at both ends of the resistor *r*. The reason why we stressed here the presence and the position of is its influence on TS properties. The length of the HV cable between the resistor *R* and the HV electrode can significantly contribute to the total capacity *C* discharging during each TS pulse. We tested different cables with lengths from 0.3 to 2 m, having capacities from

approximately 5 to 34 pF. The currents at the grounded electrode and between *R* and *r* were measured by a Pearson Electronics 2877 (1V/A) and a Pearson Electronics 4100 (1V/A) current probes. All current and HV probes were linked to the 200 MHz digitising oscilloscope Tektronix TDS2024 with a sampling rate up to 2 Gs/s.

Emission spectroscopy was used to measure the electron density from broadening of H_α line (Stark effect). For this set of experiments the input air was humidified by bubbling through water. The emission spectra were obtained using a 2-m monochromator Carl Zeiss Jena PGS2 covering UV and VIS (200-800 nm) and providing spectral resolution of 0.05 nm, coupled with an intensified CCD camera (Andor Istar) with 2 ns gate. The iCCD camera was triggered by a generator of 5 V rectangular pulses with rise time less than 5 ns. This generator was triggered directly by the discharge current signal, measured either on 50 Ω (streamer) or 1 Ω (spark) shunt. Additionally, images of single TS pulses were taken by the iCCD camera, in order to estimate the diameter of generated plasma channels. Current waveforms measured on 1 Ω shunt were identical to current waveforms measured by Pearson Electronics 2877 current probe.

III. Results and Discussion

A. Introduction to Transient Spark

When the high voltage U_{00} applied to the stressed electrode is progressively increased, we first observe a streamer corona. When the breakdown voltage is reached, a transition to transient spark occurs at the discharge voltage U_{TS}. TS is a filamentary streamer-to-spark transition discharge initiated by a streamer, which transforms to a short spark pulse (phase B, Fig. 3a). The duration of streamer to spark transition period (phase A, Fig. 3a) is from around 100 ns to several μs, depending on TS repetition frequency[30]. Figure 2 shows typical look of TS.

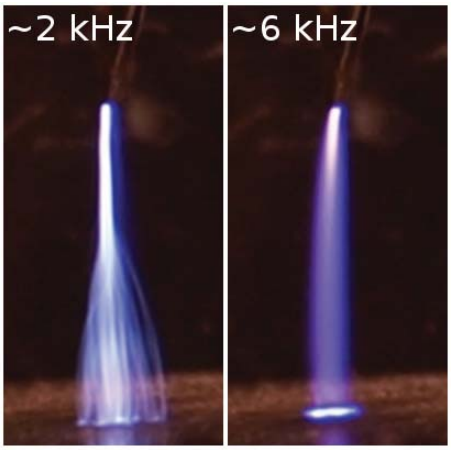

Figure 2. Photographs of TS in positive needle–plane gap of 4 mm, *R* = 6.84 MΩ, exposure 0.1 s.

The TS current pulse is due to the discharging of the capacity C, composed of several components (internal capacity of the discharge chamber C_{int}, capacity of the high voltage cable C_{cable} between the ballast resistor R and the electrode, and capacity of the HV probe C_{HV} = 3 pF). When C is discharged, the current approximately given by

$$I_1(t) \approx -C \frac{\mathrm{d}U_1(t)}{\mathrm{d}t} \tag{1}$$

reaches a high value (∼1 A) and the voltage drops to almost zero (phase C, Fig. 3a). Then, during the quenched phase (phase D, Fig. 3b), C is recharged by a growing potential U_1 on the stressed electrode. The growth of the potential U_1 in time t can be in the first approximation described by the following equation:

$$U_1(t) = U_{oo}\left[1 - \exp\left(\frac{-t}{RC}\right)\right]. \tag{2}$$

Usually, during this relaxation phase when the gap potential reaches a specific threshold, corona discharge appears, and some pre-breakdown streamers (phase E, Fig. 3a,b). A new TS pulse occurs in time $t = T$, when the voltage at the HV electrode U_1 reaches the breakdown voltage to transient spark U_{TS} (Fig. 3a), given according to (2) by:

$$U_{TS} = U_{oo}\left[1 - \exp\left(\frac{-T}{RC}\right)\right]. \tag{3}$$

From (3) we get the characteristic repetition frequency f of this process:

$$f = \frac{1}{T} = \frac{1}{RC \ln\left[\frac{U_{oo}}{(U_{oo}-U_{TS})}\right]}. \tag{4}$$

However, the repetition frequency f of the first TS pulses, when U_{00} only slightly exceeds U_{TS} is low and very irregular (Fig. 4a). Further increase of U_{00} leads to an increase of f and TS pulses become more regular (Fig. 4b). For typical R and C, the repetition frequency f is in the order of several kHz and grows with increasing U_{00} (Fig. 5). However, even with known values of C and R, formula (4) is not reliable to predict the growth of f with U_{00}, because U_{TS} also depends on f (Fig. 6). The decrease of U_{TS} with f can be explained by the increasing gas temperature T_g, resulting in a decreasing gas density N. Since some threshold, the reduced electric field E/N is sufficient to initiate the TS pulse, E and thus also U_{TS} can be lowered[30].

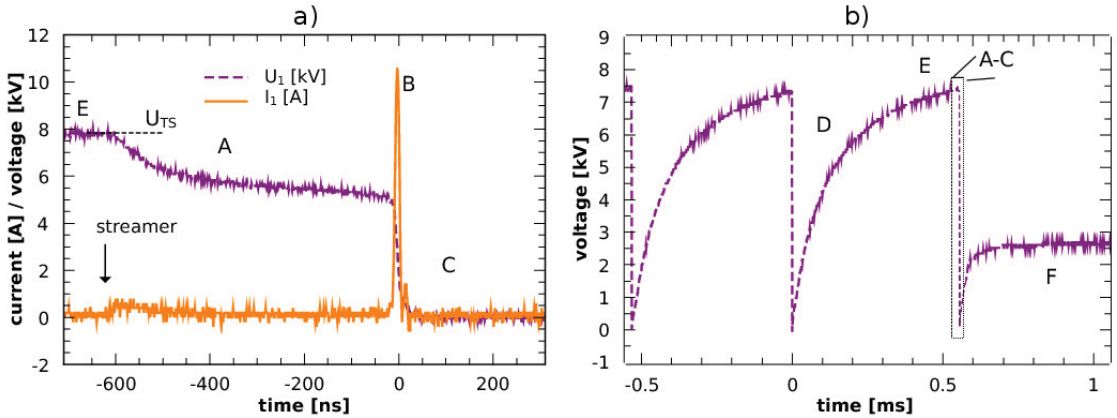

b)

Figure 3. Typical waveforms of transient spark in a) ns time scale, b) ms time scale, $R = 6.5\,\mathrm{M\Omega}$, $f \approx 2\,\mathrm{kHz}$, $r = 0\,\Omega$, $C = 43 \pm 4\,\mathrm{pF}$, $d = 5\,\mathrm{mm}$, TS pulse parameters: FWHM $\approx 12\,\mathrm{ns}$, rise and decay time $\sim 5\,\mathrm{ns}$.

The actual value of U_{TS} depends also on other parameters, the most important ones are the gap length and the sharpness of the HV electrode. In our case, it is difficult to describe the shape of the HV needle electrode geometrically. In the first approximation, its tip can be considered as an hyperboloid surface with the radius of the curvature ϕ. Although we did not accurately measure ϕ in our experiments, it is safe to say that it was between 100 μm and 1 mm. More importantly, TS does not significantly influence the shape of the tip. On the other hand, oxidation of the plane electrode has a more important influence on the TS properties. It was therefore necessary to regularly clean its surface in order to obtain reproducible results.

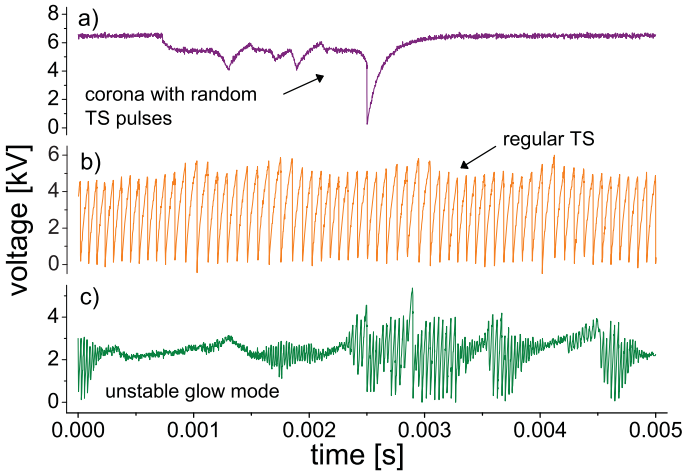

Figure 4. Voltage waveforms of different discharge regimes: a) the first random TS pulses, b) regular TS, c) unstable glow regime.

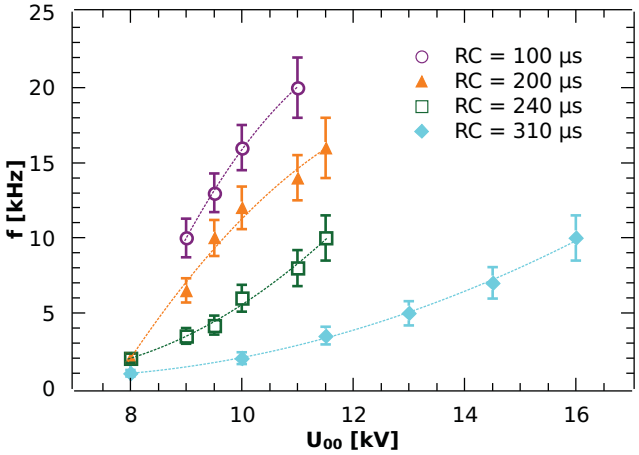

Figure 5. The dependence of f on the onset voltage U_{00} for several RC values, $r = 0\,\Omega$, $d = 5$ mm.

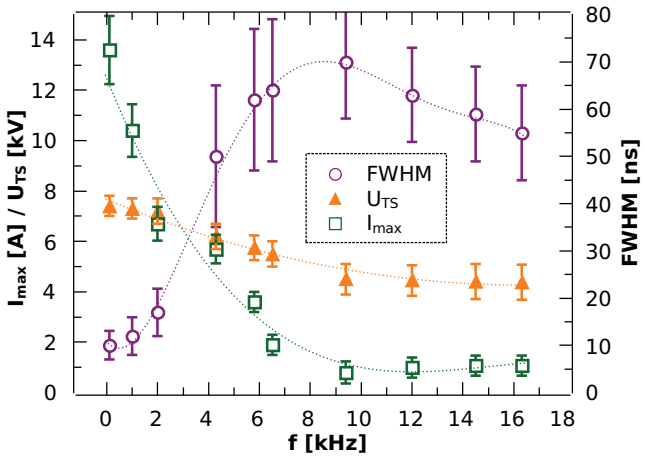

Figure 6. The dependence of peak current ($I_{\max}$), breakdown voltage U_{TS} and FWHM of current pulses on f, $C = 32 \pm 4$ pF, $R = 6.6$ MΩ, $r = 0\,\Omega$, $d = 5$ mm.

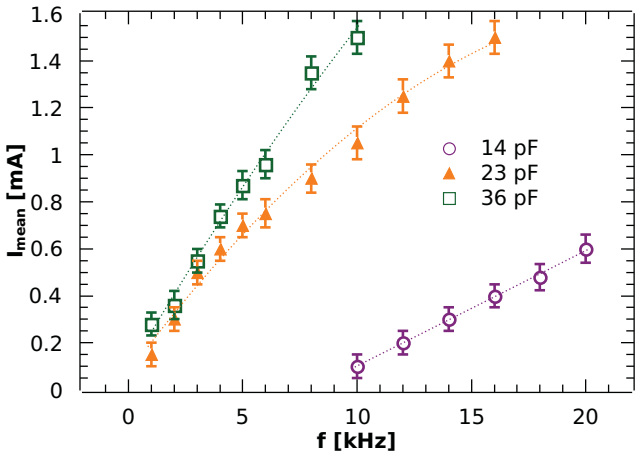

Figure 7. The dependence of mean discharge current $\mathrm{I}_{\mathrm{mean}}$ on f, $R = 6.6$ MΩ, $r = 0\,\Omega$, different values of C, $d = 5$ mm.

B. Transient spark control by electric circuit parameters

The RC term determines which frequencies can be achieved and how fast f grows with U_{00} (Fig. 5), but R and C also influence other TS properties. The major role of R is to avoid the transition to arc or the glow discharge (GD), because the increase of f is accompanied by the increase of mean current I_{mean} (Fig. 7). As I_{mean} exceeds approximately 1.5 mA, TS tends to transform into a pulse-less GD regime with a constant current up to 2 mA (phase F, Fig. 3b). However, due to the high value of R and the electro-negativity of air, this regime is not stable and the discharge randomly switches between the glow regime and the high frequency TS regime (Fig. 4c). Typically, R should be above 5 MΩ to avoid transition to a stable glow discharge. On the other hand, if $R > 10$ MΩ, the energy losses on the external resistor become too high for operating at high f and therefore also high I_{mean}. So the TS properties cannot be controlled by changing the value of R only.

The influence of C on TS is even more significant. Since TS is based on charging and discharging of C, a total charge Q_p, and the energy delivered to the discharge gap per pulse E_p are functions of C. We can therefore affect the shape of TS current pulses by changing C. Larger C typically means larger current pulses. However, we must also take into account the dependence of the current pulse maximum I_{max} and current pulse width (FWHM) on f. With increasing f, pulses get smaller and broader (Fig. 6). The increase of I_{max} with increasing C is therefore observed only at constant f.

However, the question is how to control C? It consists of several components, from which one can easily change only the value of C_{cable} by changing the cable length. Longer cable means larger C_{cable}. However, it is not very practical to change C by using different HV cables with various lengths. So we use long cables ($C_{cable} > 20$ pF) and to place a small separating resistor r between the HV electrode and HV cable. This r separates C_{cable} from $C_{int} + C_{HV}$. Like this, we were able to control the shape of the current pulse by changing r, without changing C_{cable}.

C. The influence of separating resistance *r* on TS

We expected that the increasing value of r would lead to gradual decrease of I_{max}. This tendency was experimentally confirmed (Fig. 8), but the dependence of the pulse shape and width on r was not the expected monotonous increase. We found that FWHM is not a proper parameter to describe TS pulses, since they are obviously formed by a convolution of two independend current pulses (Fig. 9). The first one (I_{C1}) is due to discharging of the capacity $C_1^{'} = C_{int} + C_{HV}$ in the gap. The second one (I_0) is due to discharging of the HV cable through the resistor r.

These two currents, I_{C1} and I_0, can explain the dependences of I_{max} and pulse shape on r. While I_{C1} does not change significantly with r (Fig. 8, 1st peak), I_0 gets smaller (Fig. 8, 2nd peak) and broader. As a result, I_{max} also decreases with r, but when the maximum of I_0 becames small compared to the maximum of I_{C1}, I_{max} remains almost constant for a further increase of r (Fig. 8, $r > 10$ kΩ). Here we obtained I_0 from I_1 after subtraction of I_{C1}. $C_1^{'}$ necessary to calculate I_{C1} was obtained by fitting measured current waveforms by (5) for large r.

We expected that I_0 can be also derived from the measured potential drop on r:

$$I_1(t) \approx I_{C_1} + I_0 = -C_1^{'} \frac{\mathrm{d}U_1(t)}{\mathrm{d}t} + \frac{U_0 - U_1}{r}. \tag{5}$$

We experimentally tested the validity of (5) by measuring current I_0 flowing through r (Fig. 10). However, the agreement between the measured current and the current calculated from U_0 and U_1 was good enough only for $r > 1.5$ kΩ. For smaller r, experimental results were in agreement only with I_0 derived from I_1 after subtraction of I_{C1}. In order to find a better formula for $I_1(t)$, which would enable us to calculate it from the measured voltage waveforms for all values of r, we performed a detailed analysis of the electric circuit representing our experimental setup.

D. Analysis of the electric circuit representing TS

Figure 11 shows a simplified electric circuit representing TS. Here, the separating resistor is characterized not only by its resistance r, but also by its inductance L_0. We found it to be crucial to explain the observed oscillations of the measured current and voltage waveforms. We even have to include the inductance L_1 of the cable from the planar low voltage electrode to ground. For this reason we also had to divide C_{int} into two parts. The first one, C_{el}, represents the capacity of electrodes. The second one is included in C_1.

The utilization of the HV probes also introduces a resistance $R_{HV} = 100$ MΩ through which a parasitic loss currents pass. The capacity of these probes is included in C_0 and C_1, respectively. The discharge plasma is represented by its resistance R_p. The plasma resistance is unknown and changes in time. This is the parameter responsible for a pulsed character of TS. If we know R_p, we would be able to describe all parameters of this circuit (U_1, I_1, ...) from the voltage and the current provided by the HV power supply. On the contrary, from the measured values of U_0, U_1 and I_1 we can derive the time variations of R_p. From R_p, we can estimate the plasma conductivity and thus the electron density.

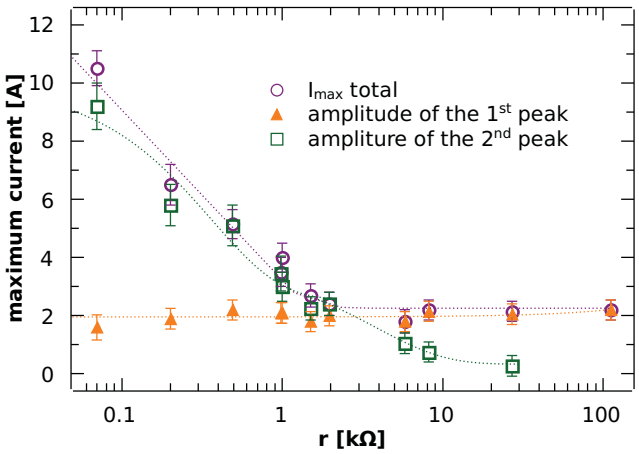

Figure 8. The influence of separating r on the amplitude of TS current pulse, and its two components, $R = 9.84\,\mathrm{M\Omega}$, $f \approx 1.1\,\mathrm{kHz}$, $C = 43 \pm 4\,\mathrm{pF}$.

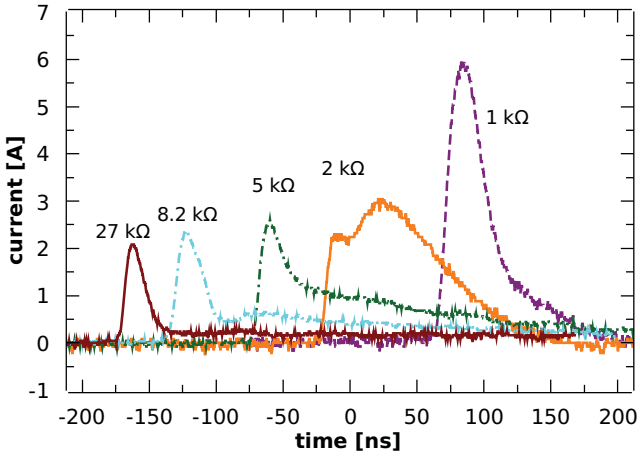

Figure 9. The influence of separating r on the shape of TS current pulses, $R = 9.84\,\mathrm{M\Omega}$, $f \approx 1.1\,\mathrm{kHz}$, $C = 43 \pm 4\,\mathrm{pF}$.

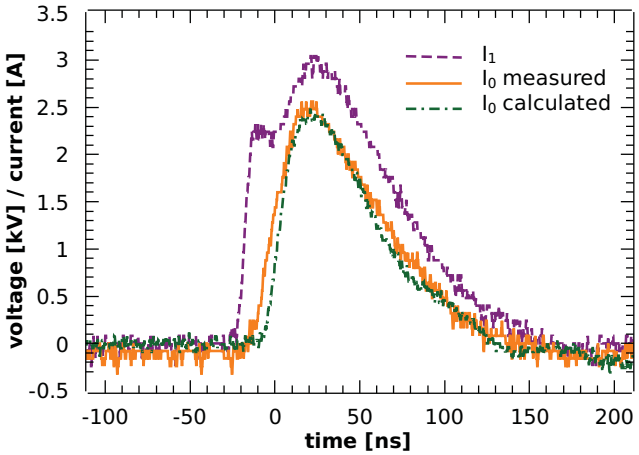

Figure 10. Comparison of I_0 measured by the current probe with I_0 calculated from U_0 and U_1, $r = 2\,\mathrm{k\Omega}$, $C = 43 \pm 4\,\mathrm{pF}$, $C_1' = 7 \pm 1\,\mathrm{pF}$.

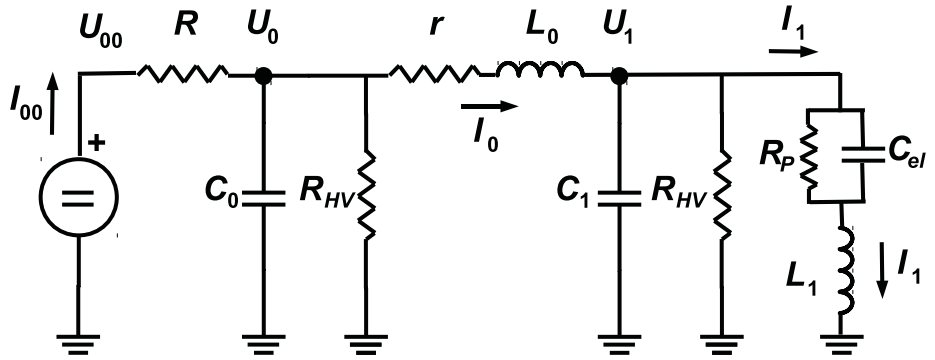

Figure 11. A simplified electric circuit representation of TS.

First of all, let us find the dependence of I_1 on U_0 and U_1 starting from the basic equations describing the electric circuit

$$I_1 = I_0 - \frac{U_1}{R_{HV}} - C_1 \frac{\mathrm{d}U_1}{\mathrm{d}t}, \tag{6}$$

$$U_1 = U_0 - rI_0 - L_0 \frac{\mathrm{d}I_0}{\mathrm{d}t}. \tag{7}$$

If r is sufficiently high compared to L_0, the third term in (7) can be neglected and from combination of (6) and (7) we get

$$I_1(t) = -C_1 \frac{\mathrm{d}U_1(t)}{\mathrm{d}t} + \frac{U_0 - U_1}{r} - \frac{U_1}{R_{HV}}. \tag{8}$$

This is actually an equivalent of the equation (5), corrected by the current lost through R_{HV}. If L_0 can be neglected, C_1 becomes equal to $C_1^{'}$, because C_{el} can be now added to C_1. If the inductance term in (7) cannot be neglected, we must use another equation obtained from the analysis of the circuit:

$$I_0 = I_{00} - \frac{U_0}{R_{HV}} - C_0 \frac{\mathrm{d}U_0}{\mathrm{d}t}, \tag{9}$$

where

$$I_{00} = \frac{U_{00} - U_0}{R}. \tag{10}$$

From the combination of (6) and (9) we get

$$I_1 = \frac{U_{00} - U_0}{R} - \frac{U_0 + U_1}{R_{HV}} - C_0 \frac{\mathrm{d}U_0}{\mathrm{d}t} - C_1 \frac{\mathrm{d}U_1}{\mathrm{d}t}. \tag{11}$$

The 1^{st} term is feeding current from the power supply, the second one is a current lost through R_{HV}. During the TS high current pulse (phase B), these two terms are negligible, but they are important to estimate the current during phases C and E. The last two terms of (11) dominate during the phase B and they correspond to two current terms in (5), but they are now both expressed as capacitive currents. Capacity C_0 is the sum of C_{cable} and C_{HV} of the 2^{nd} HV probe. Validity of this formula was again checked by fitting the measured waveforms of I_1 and I_0. For the longest 2 m HV cable we thus obtained values of $C_0 = 37 \pm 3$ pF and $C_1 = 7 \pm 1$ pF, which could be used to obtain I_1 from U_0 and U_1 for every value of *r*.

However, the problem of (11) is that it does not directly describe the dependence of TS parameters on r, which is not even included there. Moreover, we also wanted to find relations between U_0, U_1, and I_1, which would enable us to reduce the number of parameters we have to measure during the experiments. In order to reduce the number of required HV probes, we need to describe U_1 as a function of U_0. We can obtain it after we add derivative of (9) into (7):

$$U_1 = (1 + r\rho)U_0 - \frac{r}{R}U_{00} + (rC_0 + \rho L_0)\frac{\mathrm{d}U_0}{\mathrm{d}t} + L_0 C_0 \frac{\mathrm{d}^2 U_0}{\mathrm{d}t^2}, \tag{12}$$

where

$$\rho = \frac{R + R_{HV}}{R_{HV} R}. \tag{13}$$

Here we could neglect the term with the derivative of U_{00}. Finally, from the combination of (11) and (12) we get the dependence of I_1 on U_0, which also directly includes the influences of *r*, C_0, C_1 and L_0:

$$I_1 = c_{00}\, U_{00} + c_0\, U_0 + c_1 \frac{\mathrm{d}U_0}{\mathrm{d}t} + c_2 \frac{\mathrm{d}^2 U_0}{\mathrm{d}t^2} + c_3 \frac{\mathrm{d}^3 U_0}{\mathrm{d}t^3} \tag{14}$$

where

$$c_{00} = \frac{r + R_{HV}}{R_{HV} R} \tag{15}$$

$$c_0 = -\frac{rR + rR_{HV} + 2R_{HV}R + R_{HV}^2}{RR_{HV}^2} \tag{16}$$

$$c_1 = -C_0 - (1 + r\rho)C_1 - \frac{rC_0}{R_{HV}} - \frac{\rho L_0}{R_{HV}} \tag{17}$$

$$c_2 = -rC_1C_0 - \rho C_1 L_0 - \frac{L_0 C_0}{R_{HV}} \tag{18}$$

and

$$c_3 = -L_0 C_1 C_0. \tag{19}$$

The validity of (12) and (14) was also tested and confirmed by fittig measured waveforms. With equation (14), it is no more necessary to use two HV probes. However, it is crucial to measure U_0 with very low noise level, otherwise its tripple numerical derivative would lead to large error. In such a case, this equation is only useful to estimate the background and parasite currents (first two terms).

E. Estimation of the plasma resistance and electron density

We can use the dependence of the electron number density on the plasma conductivity σ_p to calculate n_e:

$$n_e = \frac{\sigma_p m_e \nu_c}{e^2}. \tag{20}$$

Here e and m_e are the electron charge and mass, respectively, and ν_c is the electron-heavy particles collision frequency. The plasma conductivity σ_p is related to the plasma resistance R_p by

$$\sigma_p = \frac{d}{R_p A}, \tag{21}$$

where d and A are the gap length and the cross-sectional area of the plasma channel, respectively.

A formula describing the dependence of R_p on the discharge voltage and current can be obtained by an analysis of the electric circuit representing TS. We get

$$R_p = \frac{U_1 - L_1 \frac{\mathrm{dI_1}}{\mathrm{d}t}}{I_1 - C_{el} \frac{\mathrm{dU_1}}{\mathrm{d}t} + L_1 C_{el} \frac{\mathrm{d}^2 I_1}{\mathrm{d}t^2}}. \tag{22}$$

From this equation, R_p can be calculated if we know values of L_1 and C_{el}. We minimized the influence of L_1 using the shortest possible grounding wires ($\sim$10 cm), with estimated inductance $\sim$100 nH. For this reason, the influence of L_1 is not negligible only for very sharp high current pulses ($I_{max} > 5$ A and pulse width $\sim$10 ns) with large derivative of I_1. These high pulses appear only at frequencies below 2 kHz, if the total capacity of the system $C >$ 20 pF and if the separating resistor r is very small ($r < 0.5\,\mathrm{k\Omega}$). For all estimates of R_p presented here can be therefore the influence of L_1 neglected. This mean that the term $C_{el} \frac{\mathrm{dU_1}}{\mathrm{d}t}$ can be also neglected, because without L_1, C_{el} can be added to C_1 and I_1 is equal to I_p.

Under these simplifications, we can estimate R_p directly from the measured U_1 and I_1, but we also used (14) to better estimate I_1 before and after the high current pulse. Moreover, U_1 is not measured accurately enough by the HV probe at the beginning of the phase B of TS, when it falls to very low values. For this reason, we estimated R_p also from I_0 and U_0, because U_0 does not drop to very low values for $r > 1.5\,\mathrm{k\Omega}$. When C_1 is already discharged, the following equation can be used:

$$R_p = \frac{U_0}{I_{00} - \frac{U_0}{R_{HV}} - C_0 \frac{\mathrm{dU_0}}{\mathrm{d}t}} - r. \tag{23}$$

Besides the uncertainty of R_p, the plasma diameter D_p, necessary to calculate A, and ν_c are another major sources of uncertainty in the estimation of n_e. We calculated ν_c in air for T_g from 300 to 1500 K and for E/N from 10 to 200 Td using our package for Monte Carlo simulation of electron dynamics[31]. We found that ν_c can vary from approximately 4×10^{11} to 4×10^{12} s^{-1}. We use the constant value 10^{12} s^{-1} to estimate n_e in TS. This approximation introduces the uncertainty of less than a factor 4.

In order to estimate D_p, we assume that plasma diameter can be well defined by the volume from which emission can be observed. We therefore performed a set of experiments of TS imaging by iCCD camera (see Fig. 12 for illustration), during which we varied the repetition frequency of TS. We defined exposure time and triggered the event to see either the emission from a whole single TS pulse (streamer + spark phase), or the emission of the streamer phase only, or the emission from the spark phase only. When we triggered the iCCD camera by the streamer current

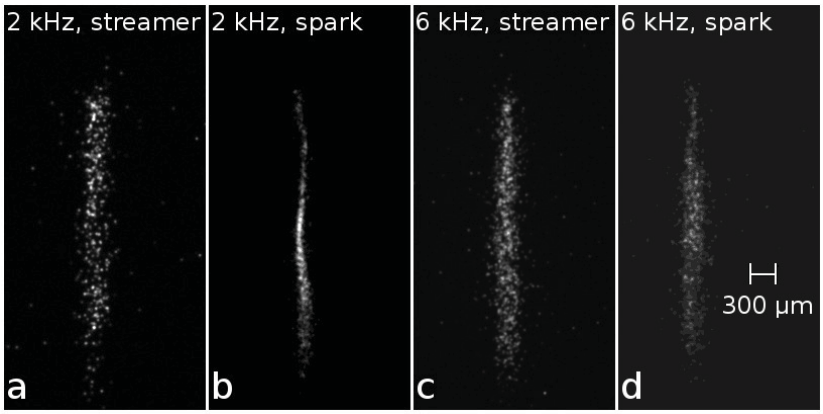

Figure 12. Images of a single pulse in different phase of TS taken by iCCD camera at two different frequencies (around 2 and 6 kHz); a) 25-175 ns from the beginning of the streamer; b, d) 25-175 ns from the beginning of the spark; c) 25-75 ns from the beginning of the streamer, $r = 0.9\,\mathrm{k\Omega}$, $R = 6.84\,\mathrm{M\Omega}$, $C = 32 \pm 4\,\mathrm{pF}$, $d = 4\,\mathrm{mm}$.

(measured on 50 Ω shunt) we imaged the whole pulse (exposure time 0.5-2 μs) or the streamer only (exposure time 25-150 ns). When we triggered by the spark current (measured on 1 Ω shunt) we imaged the spark phase only (exposure time 25-500 ns).

At lower frequencies (<4 kHz), we observed two peaks of the total emission: the first one was produced by the streamer, and the second one by the short spark. The emission during the streamer peak can be mostly attributed to the N_2(C) species, whereas the spark peak is mostly due to the excited atomic species. Images of these two phases of TS are different (Fig. 12 a,b). The spark channel is narrower (diameter up to 100 μm) and brighter than the streamer channel ($\sim$300 μm). At lower frequencies, the streamer-to-spark transition time is relatively long (up to several μs), and the diameter of the plasma channel created by the streamer shrinks before transition to spark occurs, which is in good agreement with calculations of Naidis[32]. The streamer-to-spark delay time shortens with the increasing *f*, and these two emission peaks approach each other until they merge. However, the emission from N_2(C) does not change much with *f*, while the emission intensity of excited atomic species decreases significantly, probably due to the decrease of U_{TS} and changes of the spark current profile (current pulses become broader and smaller with f). The disappearance of atomic lines explains the fact that at higher frequencies the images of the streamer phase and spark phase (Fig. 12 c,d) are very similar (diameter $\sim$300 μm). Even during the spark phase, we actually observe the emission from N_2(C) species produced by the streamer.

We also found that D_p depends on distance from the HV point electrode - it expands close to the planar electrode. Finally we decided to use a single value of plasma channel diameter $D_p = 200\,\mu$m. This is in a good agreement with a value reported by Naidis[32] from numerical simulation of the streamer-to-spark transition dynamics. Later phase of TS with current around 1 mA is similar to a glow discharge. The diameter of a stable GD channel is around 500 μm[5], and we suppose that this value can be used in the first approximation as the upper limit of TS plasma channel diameter. The approximation we decided to use therefore introduces the uncertainty less than a factor 3 for the phases A-C of TS, after the establishment of conductive plasma channel by streamer preceding the TS pulse. It is questionable whether we can approximate the plasma by a column in later phases D and E. Even if yes, its expansion should be included. Values of n_e estimated for these phases are therefore only informative. Altogether, we can estimate n_e not better than with the uncertainty of factor 10.

Figure 13 shows a typical time evolution of R_p and n_e for TS with no separating resistor r and a repetition frequency $\sim$2 kHz in two different time scales. Fig. 13a zooms on the high current phase of TS, whereas Fig. 13b shows the estimate of R_p and n_e during several TS cycles. As we can see, the initial n_e, even before bridging of the gap by a streamer, is relatively high. Values from around 10^{10} to $10^{13}\,\mathrm{cm^{-3}}$ were observed, though this value is only informative, as was mentioned above. This high concentration can be explained by preliminary streamers and corona discharge phase of TS. During the short spark pulse, R_p drops down to few hundred ohms and n_e can reach $\sim 10^{16}\,\mathrm{cm^{-3}}$. As soon as C is discharged, n_e drops quickly to about $10^{14}\,\mathrm{cm^{-3}}$. After the TS pulse, n_e gradually decreases to about 10^{10} –$10^{11}\,\mathrm{cm^{-3}}$ (Fig. 13b). In reality it should be lower, because we did not include the expansion of plasma channel in this estimation. However, even if the volume of plasma expands by two orders of magnitude (average diameter 2 mm), the lowest n_e would be in the order of 10^8 –$10^9\,\mathrm{cm^{-3}}$. In this case, the Debye length would be not larger than 0.2 mm (calculated for $T_e = 1000$ K and $n_e = 10^8\,\mathrm{cm^{-3}}$) which is by one order of magnitude smaller than the assumed plasma dimension. We can therefore suppose that plasma exists during the whole period of TS, even during the relaxation phase, although its resistance becomes quite high ($R_p \sim 10^8\,\mathrm{M\Omega}$).

Fig. 13b also shows a short period of the unstable GD regime and for this period we obtained $n_e \approx 10^{12}\,\mathrm{cm^{-3}}$. This is in a very good agreement with previous studies of GD[5], where n_e was estimated from the current density. This fact confirms that our calculated values of n_e are reasonable.

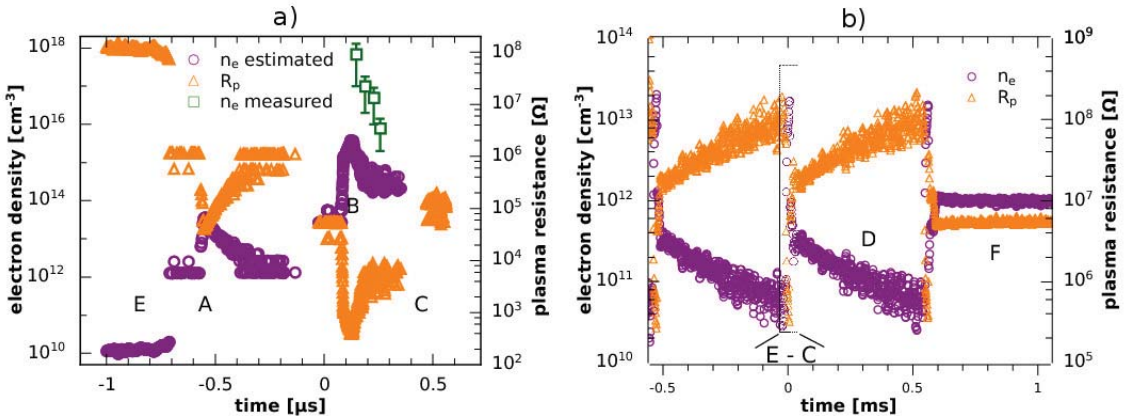

Figure 13. Calculated average electron density and plasma resistance during a TS pulse in a) μs time scale, b) ms time scale, $f \approx 2$ kHz, $C = 32 \pm 4$ pF. Figure a) also contains n_e measured by Stark broadening of H_α line near the tip of the HV electrode.

F. Influence of r on R_p and n_e

Increasing value of r leads to a decrease of I_{max} and therefore also to lower maximum n_e (Fig. 14). On the other hand, increasing r causes that it takes longer for C_0 to be discharged - up to $\sim$20 μs for $r = 111$ kΩ (Fig. 14). This prolongation of the current tail means that n_e stays relatively high longer. Typical n_e at the end of discharging of C_0 was $\sim 10^{13}$ cm^{-3}. We also estimated that it takes up to $\sim$100 μs ($r = 111$ kΩ) for n_e to drop below $\sim 10^{12}$ cm^{-3}. Thus, higher r enables to merge the characteristics of TS and GD together, i. e. relatively high current pulse ($\sim$2 A) with high efficiency of production of radicals are followed by long period with current above 1 mA, during which plasma reaches characteristics typical for GD.

On the other hand, the voltage U_0 does not drop to low values for larger r, e. g. for $r = 27$ kΩ, $U_0^{min} \approx 1.5$ kV, and so C_0 cannot be discharged completely. It is therefore not suitable to use larger values of r. The separating resistor r must remain much smaller than the ballast resistor R, otherwise the discharging of C_0 has negligible effect on the discharge current and $r + R$ can be treated as one resistor.

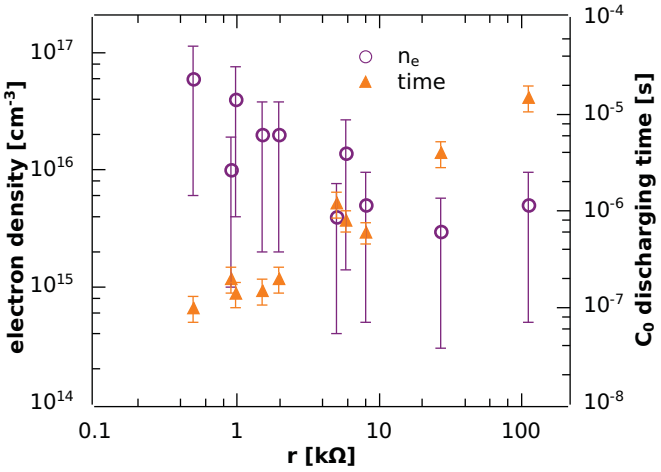

Figure 14. Dependence of maximum electron density and C_0 discharging time on r, $R = 9.84$ MΩ, $f \approx 2$ kHz, $C_0 = 37 \pm 3$ pF, $C_1 = 7 \pm 1$ pF.

G. Measurement of n_e from Stark broadening

The estimated electron density with the peak value above 10^{14} cm^{-3}, is high enough to cause Stark broadening of atomic lines of hydrogen. We therefore performed a preliminary study of Stark broadening of H_α line (656.28 nm), using humid air. The input air was simply bubbled through a vessel with water. We did not quantitatively measure the achieved humidity, but it was low that we observed no significant influence on electric parameters of TS. For this reason, the intensity of observed emission was quite weak, since we measured with exposure time only 20 ns. In this preliminary study we therefore measured Stark broadening only at low TS frequency $\sim$2 kHz, because the intensity of atomic emission lines decreased significantly at higher frequencies. Next, we also had to use H_α line instead of H_β

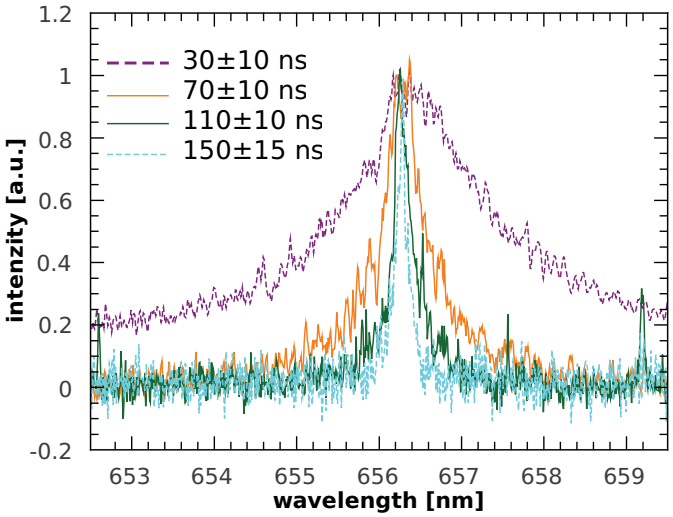

Figure 15. Normalized emission profiles of H_α line at different times after the peak of the spark current.

line, which was too weak even at 2 kHz. Calculation of n_e from full width at the half maximum (FWHM) of H_α line is difficult due to the sensitivity on electron temperature and ion dynamics. However, Gigosos et al.[33] showed, that we can avoid these difficulties using full width at the half area (FWHA) instead of FWHM and to calculate n_e by formula:

$$\Delta\lambda_{FWHA}^{H\alpha} = 0.549 \text{ nm} \times \left(\frac{n_e}{10^{23} \text{ m}^{-3}}\right)^{0.67965}. \tag{24}$$

Here, $\Delta\lambda_{FWHA}^{H\alpha}$ is the FWHA of the H_α line in nm. In order to obtain reasonable values of n_e, the FWHA must be calculated from the line profile corrected with respect to Doppler, pressure and instrumental broadening. However, the minimum value of FWHM we experimentally observed was 0.14±0.03 nm (time ∼150 ns after the peak of the spark current pulse). This value is so large, that Doppler and pressure broadening can be neglected. Even after the deconvolution of measured line profile with the slit function describing instrumental broadening, the value of this FWHM decreased to ∼0.12 nm, so the influence of instrumental broadening is within the experimental uncertainty of the measured value of FWHM. In spectra obtained in time windows closer to the current peak, with even stronger Stark broadening, the instrumental broadening can be therefore completely neglected.

Figure 15 shows normalized H_α line profiles measured in different times after the peak of the spark pulse. Calculated values of n_e are compared with estimated values in Fig. 13a. As one can see, measured n_e is at least one order of magnitude higher than the estimate. Further research is required to explain these differences. For example, we will have to measure H_α line profiles also at different distances from the tip of the needle electrode. Here we collected emission from near the tip of the needle electrode only, where n_e could be higher than the average value estimated from the plasma resistance.

IV. Conclusions

A new concept of a DC-driven pulsed discharge was investigated: transient spark, a repetitive streamer-to-spark transition discharge of very short pulse duration (∼10-100 ns) and with a very limited energy so that the generated plasma is highly non-equilibrium. This discharge can be maintained at low energy conditions (up to 1 mJ/pulse) by an appropriate choice of the resistances and capacities in the electrical circuit, and its frequency can be controlled by the applied voltage. The activity of transient spark is comparable with the nanosecond repetitive pulsed discharges but its advantage is an ease of the DC operation and no need of special and expensive high voltage pulsers with high repetitive frequency and nanosecond rise-times.

A fast iCCD camera coupled to a monochromator was used to image the discharge diameter during the streamer and spark phase. Our calculations of temporal evolution of electron density in TS based on the detailed analysis of the electrical circuit and measured plasma diameter showed that $n_e \approx 10^{16}$ cm^{-3} at maximum and $\sim 10^{11}$ cm^{-3} in average are reached. Preliminary estimation of n_e from H_α Stark broadening indicate n_e as high as 10^{17} cm^{-3} in the spark phase. Better estimation of these values requires further time and space resolved emission spectroscopic study.

The influence of a resistor r separating the HV cable from the HV electrode on the TS properties was presented here. The increasing r causes that it takes much longer to discharge the charge stored in the HV cable and the tail of the current pulse can be thus longer than several tens of μs. This additional resistor r enables to merge the characteristics of TS and the glow discharge together, i. e. relatively high current pulses (∼1 A) with a high efficiency of radical

production are followed by long periods with the current above 1 mA during which plasma reaches characteristics typical for GD. Our further research in this area will be focused on scaling up the TS discharge to produce larger volumes of non-equilibrium air plasma and to reduce the power budget.

Acknowledgments

Effort sponsored by the AFOSR, Air Force Material Command, USAF, under grant FA8655-09-1-3110, Slovak Research and Development Agency APVV SK-FR-0038-09, and Slovak grant agency VEGA, under grants 1/0293/08 and 1/0668/10.

References

[1]Civitano, L., *Non-Thermal Plasma Techniques for Pollution Control*, Vol. 1 of *NATO Series*, Springer, New York, 1993.

[2]Joshi, A., Locke, B., Arce, P., and Finney, W., *Journal of Hazardous Materials*, Vol. 41, 1995, pp. 3.

[3]Laroussi, M., *IEEE Trans. Plasma Sci.*, Vol. 30, 2002, pp. 1409.

[4]Pawlat, J., Hensel, K., and Ihara, S., *Acta Phys. Slovaca*, Vol. 55, 2005, pp. 479.

[5]Machala, Z., Janda, M., Hensel, K., Jedlovsky, I., Lestinska, L., Foltin, V., Martisovits, V., and Morvov, M., *J. Mol. Spectrosc.*, Vol. 243, 2007, pp. 194.

[6]Cernak, M., Rahel, J., Kovacik, D., Simor, M., Brablec, A., and Slavicek, P., *Contrib. Plasma Phys.*, Vol. 44, 2004, pp. 492.

[7]Loeb, L., University of California Press, Berkeley, 1965.

[8]Kulikovsky, A., *IEEE Trans. Plasma Sci.*, Vol. 25, 1997, pp. 439.

[9]Raether, H., Butterworths, London, 1964.

[10]Kobayashi, A., Osaki, K., and Yamabe, C., *Vacuum*, Vol. 65, No. 3-4, 2002, pp. 475–479.

[11]Bromberg, L., Cohn, D., Rabinovich, A., and Alexeev, N., *Int. J. of Hydrogen Energy*, Vol. 24, No. 12, 1999, pp. 1131–1137.

[12]Kanzawa, A., *Plasma Sources Sci. Technol.*, Vol. 2, No. 1, 1993.

[13]Mizuno, A., Clements, J., and Davis, R., *IEEE Trans. Industry. Appl.*, Vol. 22, No. 3, 1986, pp. 516–522.

[14]Lowke, J. and Morrow, R., *IEEE Trans. Plasma Sci.*, Vol. 23, No. 4, 1995, pp. 661–671.

[15]Penetrante, B., Bardsley, J., and Hsiao, M., *Jpn. J. Appl. Phys.*, Vol. 36, No. 7B, 1997, pp. 5007–5017.

[16]Masuda, S. and Nakao, H., *IEEE Trans. Industry. Appl.*, Vol. 26, No. 2, 1990, pp. 374–383.

[17]Walsh, J., Shi, J., and Kong, M., *Appl. Phys. Lett.*, Vol. 89, No. 16, 2006.

[18]Pancheshnyi, S., Lacoste, D., Bourdon, A., and Laux, C., *IEEE Trans. Plasma Sci.*, Vol. 34, No. 6, Part 1, 2006, pp. 2478–2487.

[19]Pai, D., Lacoste, D., and Laux, C., *IEEE Trans. Plasma Sci.*, Vol. 36, No. 4, Part 1, 2008, pp. 974–975.

[20]Pai, D., Stancu, G., Lacoste, D., and Laux, C., *Plasma Sources Sci. Technol.*, Vol. 18, 2009, pp. 045030.

[21]Pilla, G., Galley, D., Lacoste, D., Lacas, F., Veynante, D., and Laux, C., *IEEE Trans. Plasma Sci.*, Vol. 34, 2006, pp. 2471.

[22]Machala, Z., Morvova, M., Marode, E., and Morva, I., *J. Phys. D: Appl. Phys.*, Vol. 33, 2000, pp. 3198.

[23]Akishev, Y., Goossens, O., Callebaut, T., Leys, C., Napartovich, A., and Trushkin, N., *J. Phys. D: Appl. Phys.*, Vol. 34, No. 18, 2001, pp. 2875–2882.

[24]Machala, Z., Jedlovsky, I., and Martisovits, V., *IEEE Trans. on Plasma Sci.*, Vol. 36, No. 4, Part 1, 2008, pp. 918–919.

[25]Akishev, Y., Deryugin, A., Kochetov, I., Napartovich, A., and Trushkin, N., *J. Phys. D: Appl. Phys.*, Vol. 26, No. 10, 1993, pp. 1630–1637.

[26]Bastien, F. and Marode, E., *J. Phys. D: Appl. Phys.*, Vol. 12, 1979, pp. 249.

[27]Marode, E., Goldman, A., and Goldman, M., *Non-Thermal plasma techniques for pollution control*, chap. High pressure discharge as a trigger for pollution control, NATO ASI series, Part A, Springler-Verlag, Berlin Heidelberg, 1993, pp. 167–190.

[28]Hafez, R., Samson, S., and Marode, E., "A prevented spark reactor for pollutant control. Investigatin of NO_x removal," *12^{th} ISPC*, 1995, pp. 855–861.

[29]Akishev, Y., Grushin, M., Karalnik, V., Petryakov, A., and Trushkin, N., *J. Phys. D: Appl. Phys.*, Vol. 43, 2010, pp. 075202.

[30]Janda, M., Niklova, A., Martisovits, V., and Machala, Z., "Transient spark - DC driven nanosecond pulsed discharge in atmospheric air," *HAKONE XII*, Trenianske Teplice, Slovakia, September 12-17, 2010, pp. 69–73.

[31]Janda, M., Martisovits, V., Morvova, M., Machala, Z., and Hensel, K., *Eur. Phys. J. D*, Vol. 45, 2007, pp. 309.

[32]Naidis, G., *Eur. Phys. J. Appl. Phys.*, Vol. 47, 2009, pp. 22803.

[33]Gigosos, M., Gonzalez, M., and Cardenoso, V., *Spectrochimica Acta Part B*, Vol. 58, 2003, pp. 1489–1504.